Sound absorption performance of sustainable foam materials: Application of analytical and numerical tools for the optimization of forecasting models

Marco Caniato [a,*], Giada Kyaw Oo D'Amore [b], Jan Kaspar [c], Andrea Gasparella [a]

[a] Faculty of Science and Technology, Free University of Bozen-Bolzano, Bozen, Italy
[b] Engineering and Architecture Department, University of Trieste, Trieste, Italy
[c] Department of Chemical and Pharmaceutical Sciences, University of Trieste, Italy

ARTICLE INFO

Accepted 25 November 2019

ABSTRACT

Traditional models used to predict acoustic properties of poroelastic materials are usually applied to fibrous layers or polyurethane foams. However, for new materials like complex cellular foams these procedures may not be applied due to the different cell microstructure. To this aim, the sound absorbing properties of novel sustainable foam materials are investigated as a function of the nature and loading of waste powders and their effects on the microstructure and the acoustic properties. The foams are prepared from naturally occurring alginates that are in situ polymerized. The morphology and the acoustic properties of the foam-cells appear linked to the particle size distribution of the starting powder. Determination of the parameters of Johnson–Champoux–Allard acoustic model (tortuosity, viscous characteristic length, thermal characteristic length, porosity and flow resistivity) was performed using five different forecasting methods, including traditional analytical model for fibrous materials as well as inverse procedure. A new procedure for tortuosity computation of foam is proposed and validated. Transfer Matrix Method calculation of the absorption coefficient was performed and compared with the experimental data, in order to assess the validity of the model. Indirect method technique is demonstrated to be dependent on experimental measurement of thermal characteristic length.

1. Introduction

Insulation materials used in building constructions are typically organic materials made from petrochemicals or inorganic fibers made using high energy processing routes [1]. Sustainability is attracting more and more attention, accordingly use of either natural or recycled materials is desirable as it leads to energy-saving production routes, yet its industrial impact is still modest [1,2]. The recycle of inorganic materials, e.g. ceramic- or glass-based waste, though industrially assessed, generally still requires an energetic step though less demanding that the production of the starting material [3].

Among the various insulation materials, cellular foams have attracted an increasing interest of the researchers in the last 40 years, totaling about 5700 publications in the field (Fig. 1). For comparison, an impressive number of 154.700 of published patents or patent applications is recorded for the same period, signaling the strong industrial interest of such materials.

1.1. Foam production

Generally speaking, the cellular foams being porous materials, find a large variety of applications, irrespectively of their nature, wherever a light-weight porous material is needed [4]. Among them, ceramic foams find wide application, mostly as thermal and acoustic insulators [5]. Accordingly, a large amount of research is carried out in this field (Fig. 1). For such applications that generally involve macroporous material, i.e. with pore diameter higher than 50 nm, synthesis of ceramic foam is traditionally carried out by three routes: i) replica technique; ii) use of sacrificial template and iii) use of direct foaming agents [6,7]. In brief, there are some conceptual similarities in the first two routes in the sense that a precursor of the porous structures is prepared in the low temperature synthesis, either by impregnation of a "sponge-like" material or by inserting sacrificial particles as inclusions in the ceramic precursor network, followed by a calcination that removes the sacrificial material, leaving the porous cellular ceramic foam. The

* Corresponding author at: Faculty of Science and Technology, Free University of Bozen-Bolzano, Piazza Università 1, 39100 Bozen, Italy.
E-mail address: mcaniato@unibz.it (M. Caniato).

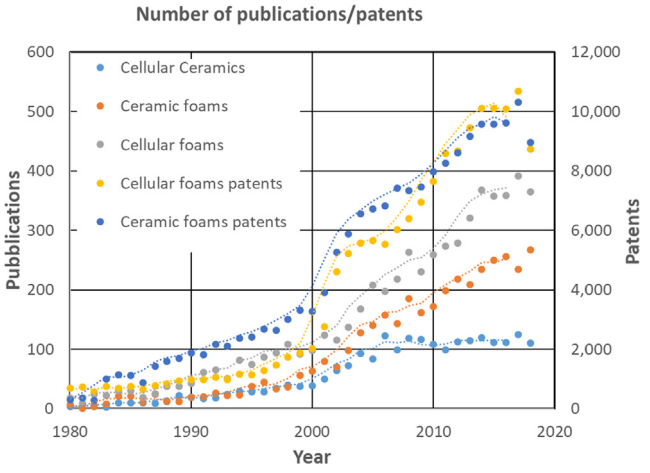

Fig. 1. Results of Scopus search using combination of the indicated keywords (search conducted in January 2019, the lines are used only as eye-guide).

advantage is that, in principle, a porous network is created in the low temperature synthesis step, which than constitutes the skeleton for the porous network generated in the calcination step. This provides a powerful tool for creating porous structures, ranging from microporous and/or mesoporous to macroporous [8]. As far as the use of foaming agent is concerned, in this case a foaming agent is added to the starting mixture which, upon calcination, generates gas bubbles in the melted material, leading to a porous structure [6,7]. Carbonates are typically used for this purpose in the industrial synthesis [9].

A common feature of all these methodologies is the necessity of a high temperature, energy demanding, calcination step, which is employed to generate the porous structure and to confer structural rigidity to the product. Furthermore, use of sacrificial reagents clearly contradicts the principles of sustainable chemistry, whereas there is an increasing need for sustainability of both processes and products [10]. In this context, use of nature derived renewable precursors and development of green production processes are of interest [10–12].

Synthesis of open cell foams based on room temperature co-gelling of alginates with glass waste as a viable and sustainable process for production of glass-based cellular foams was recently reported [13]. Alginates biopolymers have been widely investigated, mostly in biomedical applications [14,15], and have recently

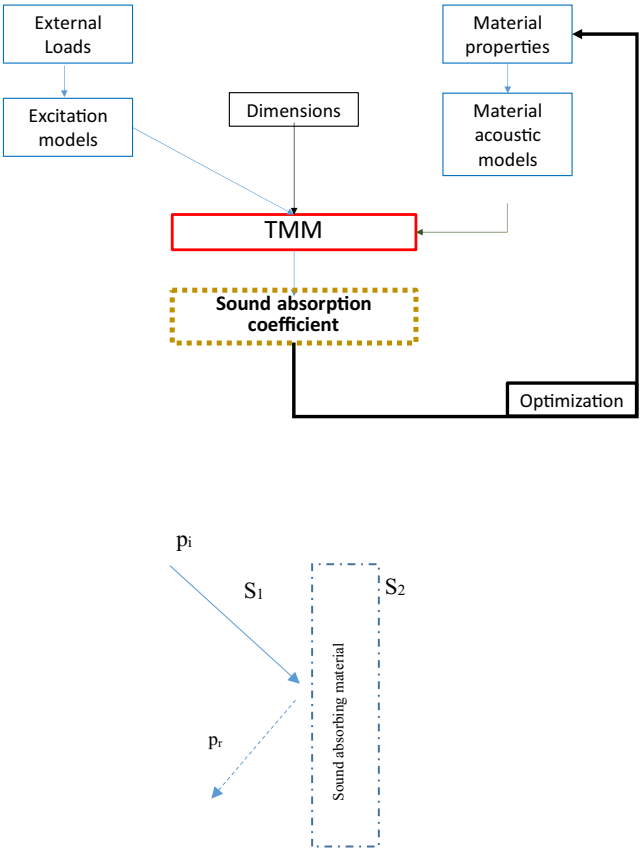

Fig. 3. Optimization TMM functional scheme (up). TMM sound wave propagation scheme (down).

attracted attention also for a number of different applications, ranging from membranes [16], fuel cell applications [17] to fire retardants and insulation materials [18]. The "foaming" principle applied for this synthesis is based on the concept of gel, which is defined by IUPAC as a "Non-fluid colloidal network or polymer network that is expanded throughout its whole volume by a fluid" [19]. This means that there is a solid porous network where the pores are filled with a fluid, which is normally liquid. Removal of the liquid to achieve the porous solid causes a significant collapse of pores due liquid surface tension, leading to aerogels, whereas gel

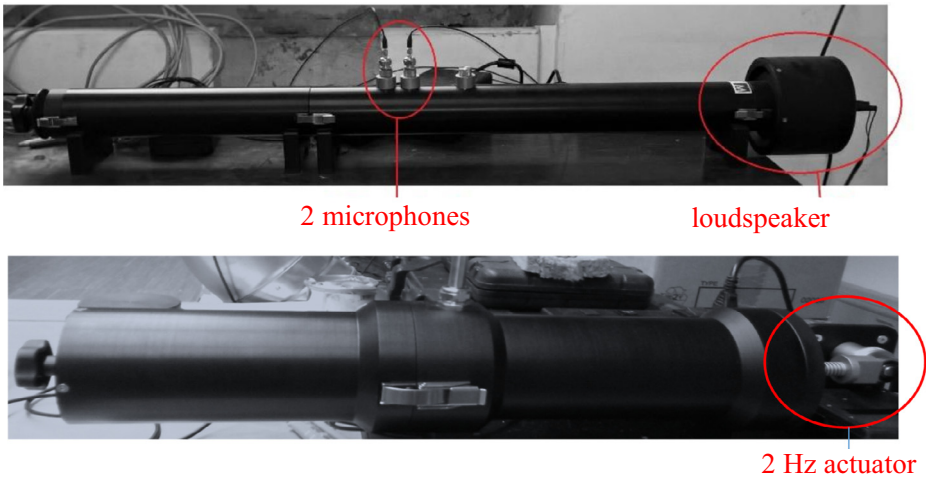

Fig. 2. Two microphones measurement test-rig with the 45 mm-diameter impedance tube (up). Airflow resistivity facility (down).

porous structure is conserved when water is removed avoiding the liquid phase, as in supercritical drying, which leads to high surface products called aerogels [20]. An alternative approach to avoid pore collapse is the use of freeze-drying technique, leading to cryogels [21]. This latter technique brings further interest elements since aligned porous structure can be achieved by directional freezing [22,23]. Consistently, alginate gels subjected to freeze-drying generate either isotropic or anisotropic pore structure depending on the freezing method [24].

1.2. Foam acoustic properties

Open-cell foams generally feature excellent sound absorption properties. For this reason, they are often used in both industry and civil sector [25], both in panels exposed to sound waves to reduce noise inside habitable volumes and in the cavity of walls, partitions, false ceilings, bulkheads, doors, etc. However, the design of these composite, complex microstructures requires a considerable amount of time and money. In fact, the choice of a right material for an application requires numerous tests, validation procedures, production of different samples with different configurations, etc. For these reasons, the availability of forecasting systems based on numerical or computational models is of paramount importance and plays a role of primary interest in all fields of applied acoustics.

Foams feature broadband sound absorption properties and consist mainly of air interrupted by a very thin solid matrix that constitutes the air cells. This particular microstructure is responsible for the foams sound absorption. In essence, the dissipation of the sound wave occurs through the interaction of the fluid with the structure, taking into account the inertia of the viscosity and the thermal characteristics. The energy is therefore partly transmitted and absorbed by the fluid and partly by the rigid material around the cell.

These aspects are responsible for the transformation of sound energy into heat, mainly thanks to viscoelastic phenomena that occur within the rigid material and in the interface between it and the fluid in motion. For this reason, the material can be considered biphasic and can be effectively modelled with the Biot theory [26–28]. According to this theory, foams can be defined as an equivalent fluid you have an equivalent density and equivalent bulk modulus according to the following equation (1):

$$\Delta p + \omega^2 \frac{\tilde{\rho}_{eq}}{\tilde{K}_{eq}} p = 0 \tag{1}$$

where $\tilde{\rho}_{eq}$ and $\tilde{K}_{eq}$ are the equivalent density and the equivalent bulk compressibility modulus and p corresponds to the acoustic pressure (the tilde symbol (~) specifies that the associated variable is a complex value and related to the frequency). According to this theory, knowledge of macroscopic parameters such as porosity, flow resistance, etc., is necessary for the model assessment.

On the other hand, for the frequency domain Johnson et al. [29] have proposed a model for porous materials with arbitrary cell shape, while Champoux and Allard [30] suggested a model to describe the thermal effects inside the porous medium.

At present, the Johnson–Champoux–Allard (JCA) model can predict frequency behavior throughout the audible range. This model depends on the following parameters:

- flow resistivity σ [N s m^{-4}],
- porosity ϕ [–],
- tortuosity α_∞ [–],
- viscous characteristic length Λ [μm]
- thermal characteristic length Λ' [μm]

Over the years, further research has been presented to improve the model on some points such as Pannetton's modification on JCA model related to the limp frame [31] or Kino's models [32], but no evidence of good agreement between predicted and measured values was proposed for complex foams, except polyurethane ones. In these cases, the foam structure could be easily compared to fibers.

Complex foams are composed of different constituents such as matrix and loading powder and represent a new sort of materials both sustainable and performant. Because of their composite microstructure, traditional acoustic procedures like inverse ones may not be effective to describe and forecast their properties. JCA based models could anyway be usable for complex foamed structures. To this end the paper discusses a modification of the analytical model and a procedure that does not imply (like traditional ones on fibers) to start from the airflow resistivity or open porosity and then use the inverse procedure, but to start from the thermal lengths and then determine the other parameters, initially blocking these first ones.

Furthermore, an attempt is made to produce some evidences about possible agreement between the traditional analytical models and complex foams. Accordingly, research is needed in order to develop predictive tools capable of reliably modelling these new materials.

1.3. Aim and scope of the present work

There is no current, theoretical or numerical model able to reliably predict the acoustic behavior of complex, non-oriented foams. In fact, theoretical models developed over the years include fibrous materials, or porous materials with cells delimited by fibers [25,33]. In previous work, a novel alginate-based cellular glass-containing foams by an alginate polymerization/freeze drying technique was developed [34] and showed that this route allows efficient incorporation of waste glass into a "green" insulation product [13].

Here the aim is to assess the following acoustic aspects: (i) to verify whether or not the available predictive models, such as the JCA model, can safely predict the behavior of an open cell complex foam thus allowing its extension to this type of materials and (ii) to assess how the modifications of the foam microstructure obtained by varying the production process conditions influence the final acoustic performance. A sample of rock wool with known characteristics is used to compare the results obtained from the foam produced in the laboratory

2. Materials and methods

2.1. Samples synthesis

Glass and fiberglass powder used to produce foams were obtained by grinding glass and fiberglass wastes using a Herzog mill with iron jar.

Alginic acid sodium salt from brown algae (medium viscosity), D-Gluconic acid δ-Lactone (GDL, ≥99.0%) and $CaCO_3$ (98%, particle size ≤30 μm) necessary for the sol–gel process were purchased from Sigma Aldrich.

Table 1
Samples characteristics and identification.

Sample	Powder precursor	Powder concentration [%w/v]	Thickness [mm]
A	Glass	10	11
B	Glass	20	11
C	Fiberglass	20	11

The foam synthesis process is based on the incorporation of a powder into an alginate composite hydrogel, which is then freeze-dried [34]. The principle is that after the initial formation of a three-dimensional porous hydrogel network, the cells are formed in the freeze-drying step as the water entrapped in the gelation is removed by sublimation, obtaining a porous structure [35].

The powders (glass or fiberglass) in appropriate ratios (Table 1) were dispersed in an alginate-containing aqueous solution and the in situ gelation was then carried out by adding GDL and $CaCO_3$. In this way the calcium cations were slowly released from $CaCO_3$ when the pH of the aqueous solution gradually decreased as a consequence of GDL hydrolysis in water [36,37]. The gelation of alginate-based solutions is due to the calcium ions that preferentially bind to the G-blocks of the polysaccharide in a highly cooperative manner, resulting in ionic crosslinking.

Petri dishes with a diameter of 90 mm were used to obtain gels with a final volume of 88 ml. Once gelled, the samples were freeze-dried for ca. 24 h.

Freeze-drying was implemented in an Alpha 1–2 LD Plus freeze drier, connected to a vane pump (Vacuubrand RZ 2.5).

Table 1 describes the samples synthetized and used in this work, which were prepared under optimized gelation conditions by varying the nature of the powder and its concentration.

2.2. Samples characterization methods

2.2.1. Compression tests

Compression tests were performed with a Shimadzu Autograph 2, AG-10TA equipped with a 500 N load cell. A constant compression speed of 2.5 mm/min was used according to the ASTM D1621 (ASTM 2000) and the compression modulus E_c was determined from the load–displacement curves: deformation could be considered linear from 0.03 to 0.08 mm. Tests were performed on five specimens for each type of foam sample and on five specimens of 150 kg/m^3 rock wool with an average diameter with an average diameter of 28.9 mm and an average height of 25.4 mm.

2.2.2. Microscope and image analysis

Foam microstructure pictures reported in Fig. 4 were collected using a Leica-Stereoscan 430i Scanning Electron Microscope (SEM). Samples were sectioned and analysed by SEM after Au sputter coating.

Image J software was used for image analysis in order to evaluate the size of foam cells and FME workbench to evaluate porosity.

2.2.3. Acoustic experiments

Cylindrical samples with a diameter of 45 mm were produced and acoustic parameters (absorption coefficient and impedance) were measured using an impedance tube with a 45 mm diameter according to ISO 10534-2:1998. A two microphones with hard backing configuration was used as shown in Fig. 2 using a loudspeaker as noise source. The measurements were performed between 100 Hz and 4000 Hz using a sine swept signal. Tests were done on three specimens for each type of foam sample of 11 mm thickness and on three 150 kg/m^3 rock wool samples of same thickness.

Airflow resistivity was measured using a 2 Hz alternative air flux, computing the value on the effective value (Fig. 2).

2.3. Acoustic numerical simulation

2.3.1. Acoustic model parameters

From an analytical point of view, flow resistivity, porosity (ϕ), tortuosity (α_∞) and characteristic lengths (Λ,Λ') can be determined according to the following relationships (Eq. (2)–(5)), representing the current state-of-the-art for general modelling of JCA parameters [38]. Their general assumptions are related to periodicity of the microstructures, very small Knudsen number values (ration of the gas molecular size and a characteristic pore) and interconnected pore structures.

$$\phi = 1 - \frac{\rho_m}{\rho_b} \tag{2}$$

$$\alpha_\infty = 2 - \phi \tag{3}$$

$$\Lambda = r_0 \frac{\phi(2-\phi)}{2(1-\phi)} \tag{4}$$

$$\Lambda' = r_0 \frac{\phi}{1-\phi} \tag{5}$$

where ρ_m is the overall density of the sample and ρ_b is the bulk material composing the open cell. For the air flow resistance the most used model is Tarnow's one [39]:

$$\sigma = \frac{4\pi}{b^2(-0.64\ln(d) - 0.737 + \mathrm{d})} \tag{6}$$

where η is the air viscosity, b is or square root of area per fiber and d the volume concentration of cylinders.

The acoustic model parameters were calculated form the Eqs. (2)–(6) using experimental data (SEM measurements, etc.) and then employed as input values for the Transfer Matrix Method (TMM) calculation of the acoustic absorption coefficient. The use of these analytical model is explained by the fact that these are the most used and simple predicting equations found in literature. Thus, an attempt to understand if they could work also with complex foams is of paramount important. If this case will not be verified, then a proposal for their modification will be provided.

2.3.2. Acoustic indirect method

Direct measurement of all fluid phase parameters (e.g. airflow resistivity, open porosity, tortuosity, viscous and thermal lengths) requires a set of test-rigs to be used and can be difficult to perform. As an alternative, inverse identification methods, which is used here, allows evaluating these parameters from the acoustical measurements in a standing wave tube.

Using the experimental data, a minimization procedure (based on a non-linear best-fit approach) is implemented in order to determine 5 physical parameters that minimize the difference between the experimental test and the analytical model. For this simulation ICT_MAA software is used (http://www.materiacustica.it/mat_Software_ICT.html).

The five parameters related to the fluid phase, were determined by applying an inversion procedure algorithm to experimental laboratory acoustic measurements [40–41].

2.3.3. Acoustic TMM numerical simulation

A Johnson–Champoux–Allard (JCA) model was implemented using TMM. This procedure deals with a mathematical matrix approach where many dedicated models could be introduced when needed and solved in an all-inclusive one (Fig. 3 up).

More specifically, TMM generally solves a two-dimensional problem related to the impact of a flat acoustic wave on the surface of a structure composed of two or more layers. In general, the method can be described analytically as follows (Eq. (7)):

$$\mathrm{V}(\mathrm{S}_1) = [\mathrm{T}]\mathrm{V}(\mathrm{S}_2) \tag{7}$$

The vector $V(S_1)$ represents all the variables necessary to define the acoustic indicators (pressure, stresses, velocity, etc.) present on the surface S_1, while the vector $V(S_2)$ contains the same descriptors for the surface S_2 (Fig. 3 down). Elements of matrix T depend on physical and mechanical parameters relative to each specific layer.

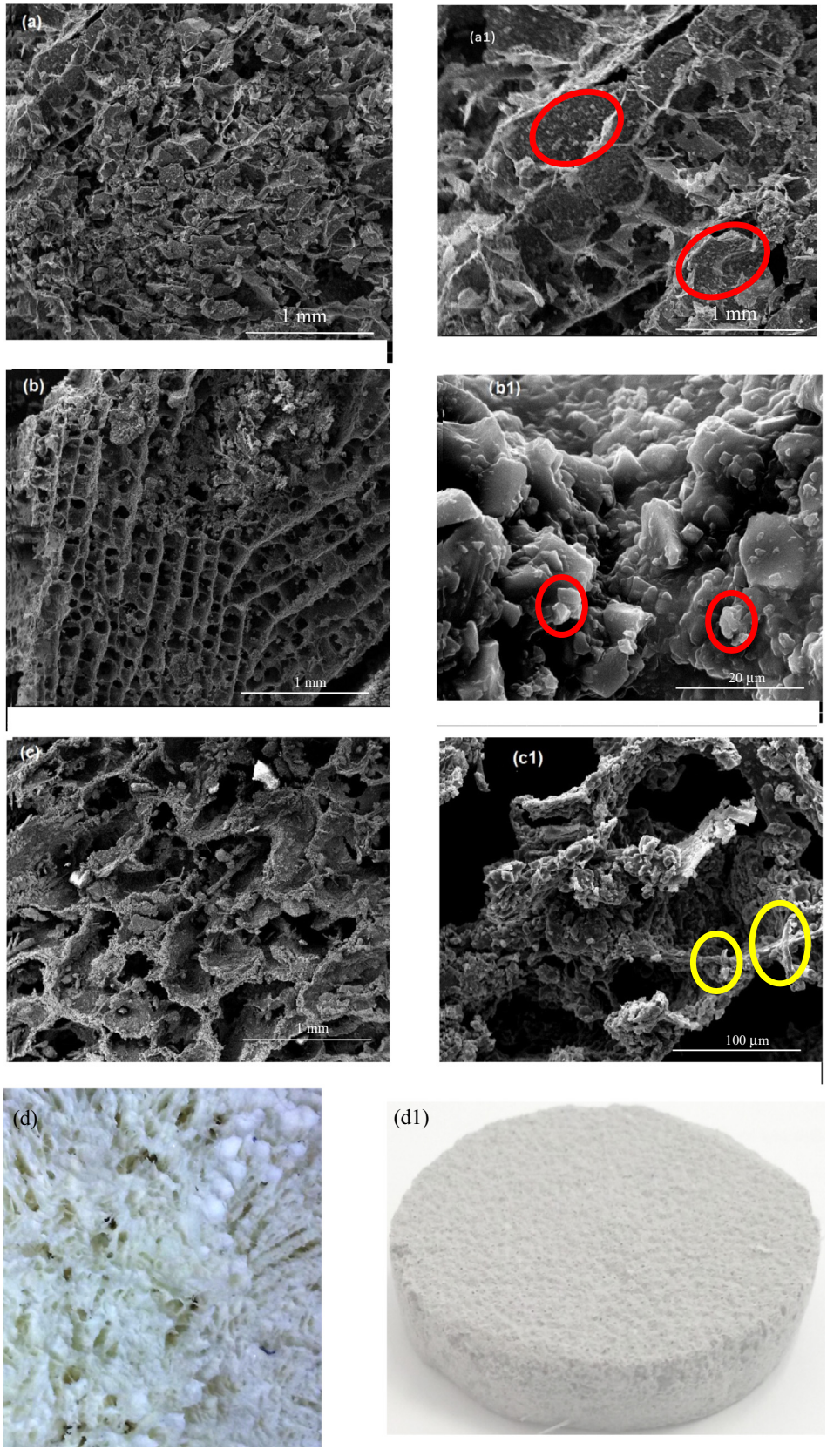

Fig. 4. Pictures of the produced complex foam. SEM pictures: (a) sample A 50x; (a1) details of sample A 50x, evidencing some of the glass powder inclusions; (b) sample B 50x; (b1) details of sample B 2500x evidencing some of the glass powder inclusions; (c) sample C 50x; (c1) details of sample C 500x evidencing some of the fibreglass inclusions. (d) Macrostructure of sample A; (d1) sample C.

In other words, the transfer matrix [T] describes the full transmission of sound waves through the layered structure. The size of this matrix depends on the nature of each layer, such as solid, fluid, poroelastic or viscoelastic.

Assuming that the layered structure is enveloped in a semi-infinite fluid on both sides (hard-wall boundary condition), it is possible to describe the complex reflection coefficient is defined as follows (Eq. (8)):

$$R = \frac{Z_s \cos\theta - Z_0}{Z_s \cos\theta + Z_0} \tag{8}$$

where $Z_0 = \rho_0 c_0$ represents the characteristic impedance of the fluid. This is a function of density ρ_0 and speed of sound c_0 and θ is the incidence angle that is equal to zero, for sound absorbing coefficient measured at normal incidence. Z_s represents instead the surface impedance of a layer of the package considered and can be calculated as follows (Eq. (9) and Eq. (10)):

$$z_s = \frac{\det[D_1]}{\det[D_2]} \tag{9}$$

and

$$\alpha(\theta) = 1 - \left|R^2\right| \tag{10}$$

being D_1 and D_2 matrices obtained from a complete matrix D (combination of transfer matrix of each layer, coupling matrices and proper boundary conditions) and $\alpha(\theta)$ the sound absorbing coefficient calculated for any θ angle.

3. Results and discussion

3.1. Foam microstructure and mechanical properties

Our previous investigation showed that alginates as gelation agent incorporate recycled glass powders leading to open cell foam structures when the freeze-drying process is applied to the starting gel. Since the intent of this research is to understand the influence of the coarse foam structure, no bonding agent with these functions was added. As a matter of fact, natural bonding agents with function of aggregators and plasticizers like organic compound were used in order to obtain flexible panels as well as rigid ones [37,42–44], containing composite materials (or waste) and composite polymeric materials (or wastes) as dispersed powders. If the specimens are flexible, an improvement (or no differences compared to rigid one)) of the sound absorption properties can be obtained for medium high frequencies [45].

As described in Section 2.1, using the optimized synthesis conditions, three samples A, B and C have been prepared containing respectively 10 and 20% w/v of glass powders and 20% w/v of fiberglass. Fiberglass is a difficult and costly to recycle thermoset composite [46,47], which makes of interest its use as a foam component, as a possible, environmentally friendly, recycle route. Fig. 4 reports the micro-structure of the as synthesized samples, the macrostructure is exemplified for sample A as no significant change is observed for specimens B and C. A macroporous open cell morphology is observed for all the samples, confirming the efficiency of the proposed methodology for preparing cellular foams.

Table 2
Average area of the foam pores.

Sample	A	B	C
Pore medium area [mm^2]	0.011	0.019	0.074
Standard deviation [mm^2]	0.011	0.009	0.033
Radius mean value [μm]	29	38	75
Porosity	0.85	0.91	0.93

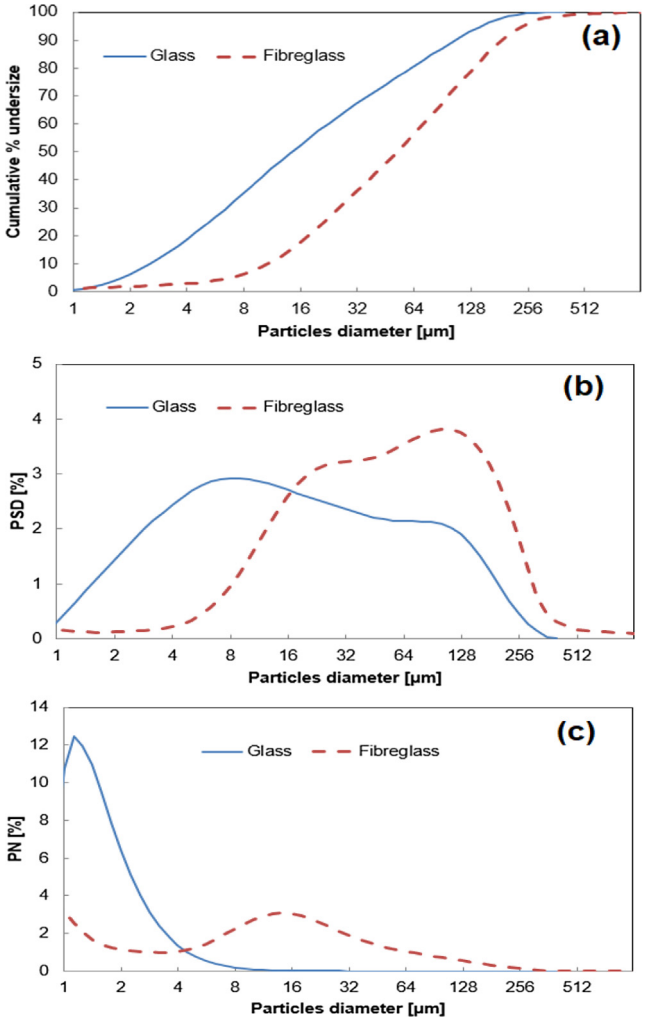

Fig. 5. Granulometric analysis of glass and fiberglass powders: (a) cumulative % undersize; (b) PSD; (c) PN.

As shown in Fig. 4(a)–(c), taken at higher magnifications, both glass and fiberglass are well dispersed and engulfed within the cell walls made of the alginate polymer.

Remarkable is the change of the shape and alignment of the pores as the amount and nature of the solid additive is varied (Fig. 4(a)–(c), Table 2). Both glass containing samples A and B mostly feature a quadratic/rectangular form the cells, the increase of the amount of glass powder from 10% w/v to 20% w/v promotes orientation of the cells and increases the pore dimensions. By substitution of the glass with fiberglass, the orientation of the cell is lost and pores are slightly larger with respect to sample B. These observations suggest the presence of a clear interplay between the gelling agent, the powder and the freeze-drying process.

As for the powders, Fig. 5a reports the cumulative percentage undersize plot for the glass and fiberglass particles from which the particle size distribution (PSD) curves, expressed as weight percentage (Fig. 5b), and particle number (PN) percentage (Fig. 5c) were derived assuming a spherical particle geometry. As for the weight-based PSD, the glass powder features smaller particles on average, the PSD peaking around 8 μm for glass while around 128 μm for the fiberglass (Fig. 5b). Consistently, fairly large, submillimeter, glass-fiber particles are detected in the SEM micrographs; some of them are indicated by arrows in the Fig. 2c. Importantly, PN clearly shows that about 90% of the glass particles

feature a particle size minor than 4 μm in the glass powder, which increases to ca. 60 μm for the fiberglass powder (Fig. 5c).

Generally speaking, freeze-drying synthesis is strongly affected by the process conditions: for example, directional freezing efficiently oriented the growth of the ice particles in a single direction, leading to monolith type of morphology [23,48]. This technique could be applied also to alginate-containing gels leading to anisotropic products [24]. Having employed uniform freezing conditions, this effect is not expected to be responsible for the observed oriented morphology of sample B. The amount of doping powder and their particle distribution seem to provide a key for the interpretation of our results: it seems reasonable to assume that the effect of the particle size and number becomes more important in the ice freezing process as the amount of the glass component increases passing from sample A to B. The principle of ice templating is that, during the crystallization, rejection of the suspended particles/gel from the ice crystals occurs, leading to a specific morphology dictated by the crystallized solvent [49]. Ice nucleation is essentially a heterogeneous process which is favoured by small particles as they provide a large number of nucleation centres [50,51]. Thus the huge amount of small particles in sample A compared to B shown in Fig. 5c provides an interpretation of the results: high amount of very small particles favours an increase of the ice front velocity which would promote formation of a columnar ice front that easily accounts for the glass-containing samples A and B morphology [52]. At a comparable solid material loading, sample C contains less small particles given their larger average dimension, the rate of nucleation decreases to produce an isotropic pattern of the open cells, which, however, presents larger dimension consistent with the higher particle size [49,50].

As far as the density and the compression modulus are concerned (Table 3), the observed trend seems to correlate with the dimension and hence number of the open cells in a fixed volume: higher the pore area, lower the number of cells. Accordingly, density increases in the sequence: sample A, B and C, whereas the opposite occurs for the compression modulus.

3.2. Acoustic performance and analytical model

Fig. 6 reports experimental sound absorption coefficient for samples A, B and C. Samples A and B show similar behavior even if sample B offers greater global sound absorbing properties compared to A: the highest absorption coefficient observed for sample B is 0.998 at 2190 Hz, which then rapidly declines. It appears clear that sample C behaves differently from A and B with a maximum of absorption peaking at about 2100 Hz followed by a slow decline. These results appear in line with the different morphology of sample C compared to A and B thus leading to different acoustic properties. Consistently, the comparable performances of samples A and B are in line with the observation that both glass-containing samples feature a similar type of oriented morphology as clearly evidenced by the SEM pictures (Fig. 4a, a1 and b).

Due to production technique and difficulty of properly adapting the samples to the tube, there were some leakages that would not provide reliable results above 3000 Hz. So, it was decided to limit all the graphs to this more relevant frequency range.

Table 3
Density and Compression modulus.

Sample	Density [kg/m^3]	E_C [MPa]	Standard deviation [MPa]
A	186	5.2	0.6
B	201	4.2	0.3
C	250	3.4	0.1
Rock wool	150	1.0	0.1

Thus, the experimental determination of the sound absorption coefficient clearly reveals a different capability of the samples where the sample C performance results quite different compared to samples A and B, showing a clear consistency of both microstructural and acoustic properties.

In order to model the sound absorption coefficient, the five parameters were calculated according to Eqs. (2)–(6) using the measured densities and the thickness of the cells evaluated from the SEM micrographs (Table 4).

The frequency trends of the sound absorption coefficient, which were calculated using these parameters as input for the TMM procedure, are shown in Fig. 6.

The trends reported for materials A, B and C clearly show an unsatisfactory agreement between the calculated and experimental data demonstrating that the analytical model procedure as implemented using the Eqs. (2)–(6) does not provide a reliable model for the complex foam structures. On the contrary, a reasonably good fit is obtained when the rock wool is modelled, which is consistent with the general assessment of the application of this methodology to fibrous materials [32,39]. An attempt was therefore made to extend this model to the considered foams, in order to obtain more reliable prediction of their sound absorption coefficient.

The microstructural data presented in Section 3.1 show the possibility of changing the internal morphology of the foam by controlling the addition of the glass-containing powder, both by modifying the quantity and particle distribution. The powder is incorporated into the walls of the cells, which results in an extension of the free path that the wave can make within the material itself. By increasing the powder percentage (from Material A to Material B) this path will increase. For this reason, by modifying the tortuosity parameter, the sound absorption can be modified, without changing the thickness of the material. The equation (11) is therefore proposed as a partial modification of the Eq. (3), which is able to provide a more a reliable fit, up to 2500 Hz, for materials A and B which extends to the whole frequency range for material C, modifying the formulation of Archie for the tortuosity [53], because this model depends only on the open porosity:

$$\alpha_{mod,\infty} = \frac{1}{\phi^{12.72}} \tag{11}$$

The exponent of the open porosity is calculated by a curve-fitting procedure of all measured results. The values of the tortuosity calculated using Eq. (11) are included in Table 4. The results of absorption coefficient modelling using the modified tortuosity Eq. (11) are reported in Fig. 7, which show a nice agreement between the experimental and modelled data. Accordingly, the "traditional" analytical model (Eq. (3)) will not considered further.

A comparison of the data reported in Figs. 6 and 7 clearly indicates the crucial importance of the tortuosity factor in determining the sound absorption capability of these materials: it is important to highlight that this is the only parameter out of five which changes in the two modelling.

3.3. Acoustic indirect method

As discussed, the modelling of the acoustic properties of porous materials requires to determine physical parameters of the porous solid, namely airflow resistivity, open porosity, tortuosity and viscous and thermal characteristic lengths [54]. As an alternative approach, an inversion method can be applied which consists in a best fit procedure of the experimental acoustic data to provide all these parameters as the output [40]. Such an approach could successfully be applied to a number of different types of porous materials [55]. This is exemplified in Fig. 8 which reports the

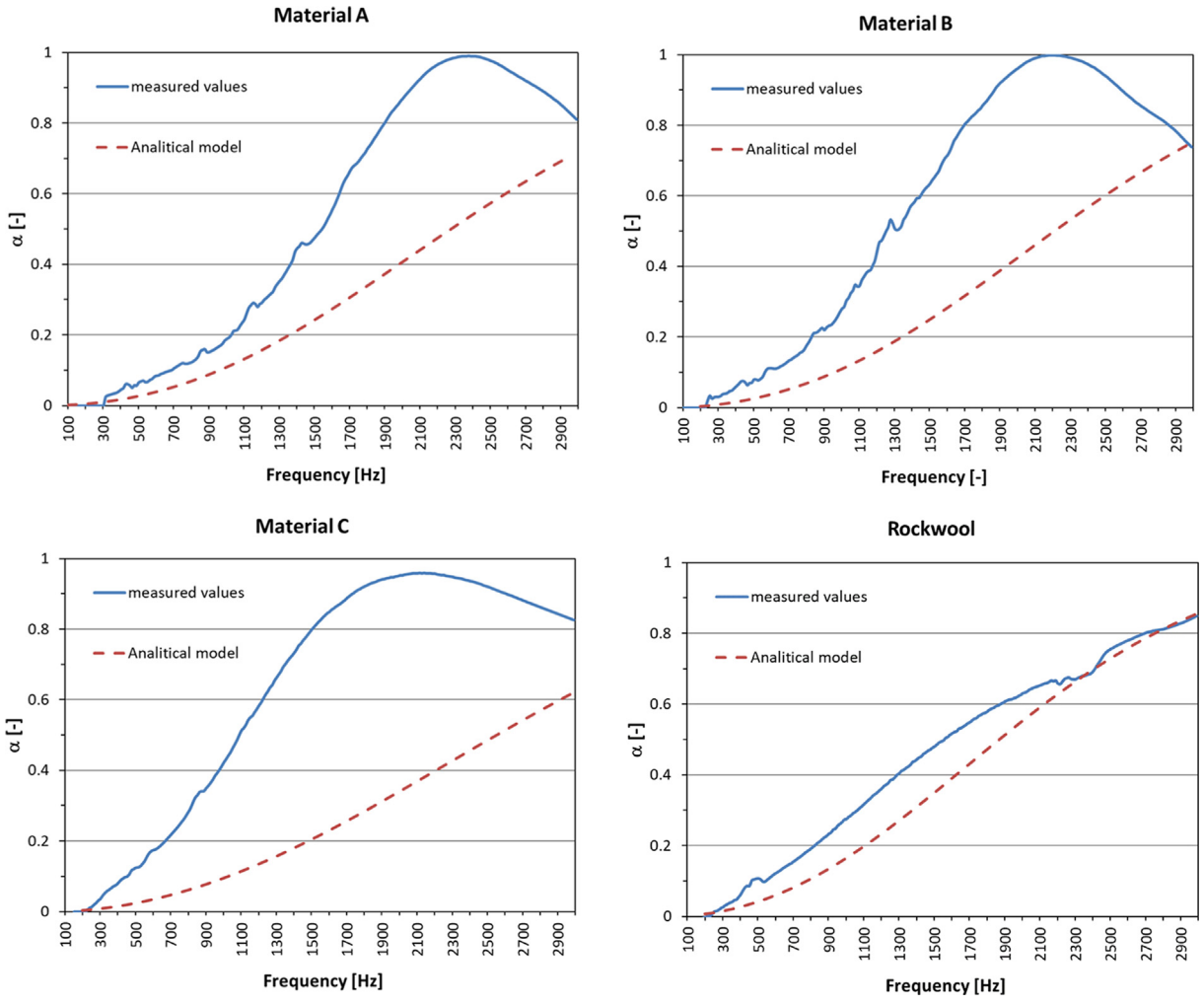

Fig. 6. Sound absorption coefficient as a function of frequency: Analytical model (calculated with TMM) vs. experimental values.

Table 4
Analytical model results: flow resistivity, porosity (ϕ), tortuosity (α_∞) and characteristic lengths (Λ,Λ') calculated using Eqs. (2)–(6) and (11).

Material	Flow resistivity (Eq. (6)) (σ) [(N s) m^{-4}]	Porosity (Eq. (2)) (ϕ) [–]	Tortuosity (Eq. (3)) (α_∞) [–]	Tortuosity (Eq. (11)) (α_∞) [–]	Viscous characteristic length (Eq. (4)) (Λ) [μm]	Thermal characteristic length (Eq. (5)) (Λ') [μm]
A	24,428	0.92	1.07	2.89	31	57
B	27,648	0.91	1.08	3.33	28	52
C	39,526	0.89	1.1	4.41	23	41

comparison between the measured and calculated trends for a free inversion of the rockwool sample.

The inversion procedure algorithm was therefore applied to the experimental acoustic measurements using three different approaches: In the first one, no restriction has been applied to the inverse procedure. In the second one, restrictions were applied with the aim to achieve the best fit, based on the results of the analytical modified model. The limitations were applied in terms of upper and lower limits of the flow resistivity (σ) within which the inverse procedure can fit. In the third one, the thermal characteristic length (Λ') value was imposed based on the experimental data (pore radius in Table 2) in the inverse procedure. The choice of these restrictions is motivated by the fact that these parameters are those usually experimentally measured in respectively acoustic and material science studies.

Figs. 8–10 compare the measured sound absorbing coefficient frequency trends as well as the complex impedance for the three materials with the calculated ones (with TMM). A perusal of these figures discloses a quite good agreement between the fitted and experimental curves, suggesting that an appropriate fit has been obtained for all the three approaches employed, unrestricted fitting giving the best result (compare for example sample A).

To evaluate the goodness of the fit, a standard deviation calculated by considering the experimental values (average of three measurements) as the average value (μ) for each frequency and the modelled data as experimental ones (Eq. (12)):

$$\sigma = \sqrt{\frac{1}{N}\sum_{i=1}^{N}(x_i - \mu)^2} \tag{12}$$

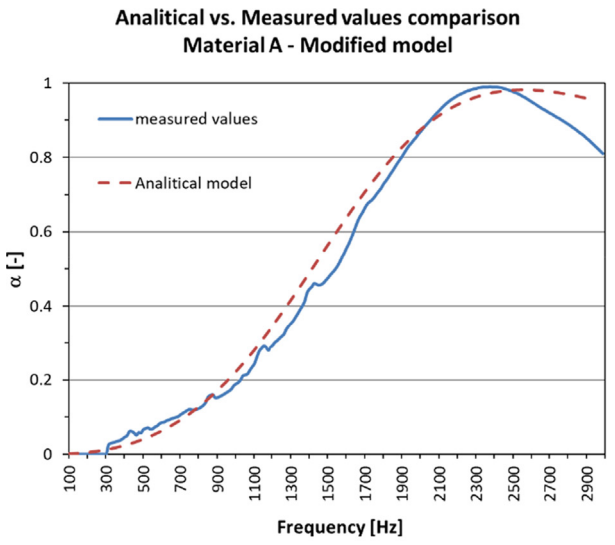

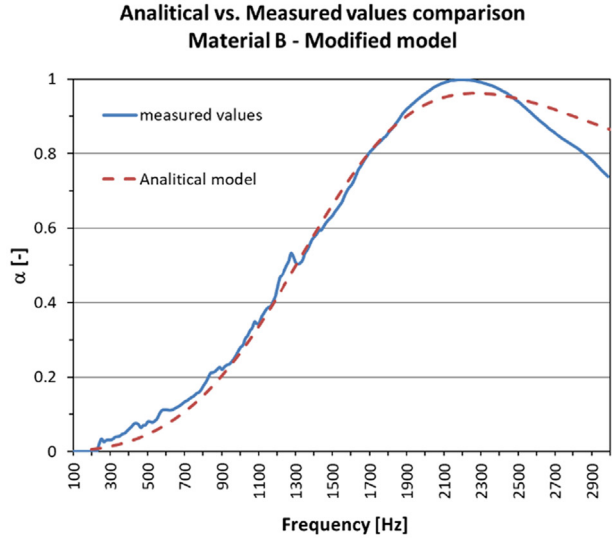

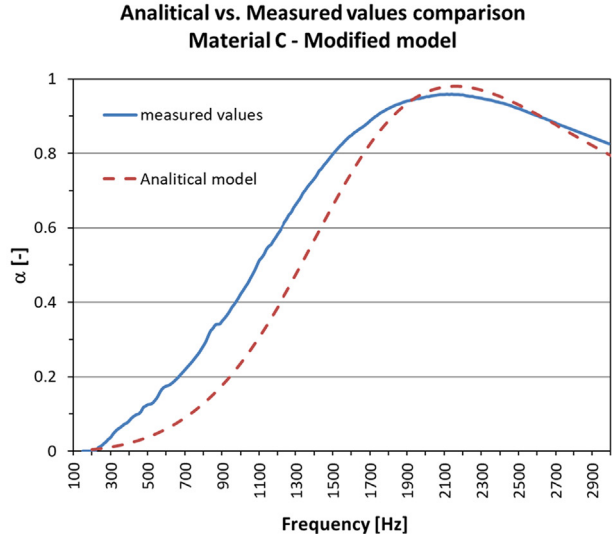

Fig. 7. Sound absorption coefficient as a function of frequency: Modified analytical model, using Eq. (11) (calculated with TMM) vs. experimental values.

The deviation thus calculated clearly shows: (i) minor effects of the restriction on the parameters on the goodness of the fit upon variation of the fitting procedure; (ii) unrestricted fit is slightly better than those restricted; (iii) the fit for samples A and B results significantly better compared to sample C. As for the latter aspect, the microstructure investigation (Fig. 2) shows a more regular cell morphology in the case of the glass-loaded foams whereas the morphology sample C has somewhat irregular pore morphology. Accordingly, the fitting procedure, based on an idealized structure, fits better regular structures compared to those irregular.

3.4. Comparison of the results

Summarizing the results, four different parameter sets have been derived by the above described procedures (Tables 3 and 5). These were used to calculate the TMM-based forecast of the sound adsorption capability and compared with the experimental data (Fig. 11).

As a general observation, using the parameters calculated in the modified analytical model, the calculated TMM profile fits worse the experimental data compared to those obtained by the inverse method. Consistently, calculation of standard deviation respectively for samples A, B and C resulted in values of 0.741, 0.557 and 1.568, significantly higher than those calculated for the inverse method (Table 5).

As for the inverse method, it was already noticed that the "free parameter" inverse fitting provides the best fit. However, it is important to relate the derived ϕ,α,Λ and Λ' parameters to the real microstructure of foam materials in order to discriminate the proper fitting model out of the four considered.

To facilitate this task, Fig. 12 reports the comparison of the obtained acoustic parameters for the four sets expressed in terms of relative percentages. A perusal of the Fig. 12 reveals a number of significant features. By considering the comparison in terms of the samples, the behavior of samples A and B clearly differs from that of sample C in terms of concordance of the results of the different procedures. This is consistent with the significant difference in the morphology of sample C with respect to samples A and B.

Specifically, sample C features very minor differences for the parameters σ, ϕ, and α whereas the parameters Λ and Λ' calculated for the modified analytical model result about half of those calculated by the other procedures. As discussed below, these parameters are linked to the physical nature of the cellular structure which can account for the underestimation of these values given the different nature of these material as, compared to those usually investigated [55].

As for the materials A and B is concerned, a remarkable disagreement between the "free fit" inverse method and all the other procedures is found for the α, Λ and Λ' parameters. This may be taken as clear evidence that a local minimum has been achieved in this fitting [40,55], which, however, is irrelevant to the physical nature of these samples (see below).

Noticeably, the tortuosity obtained by modified analytical method well compares to those obtained from the inversion method using the value of the fixed Λ' parameter. Being this method based on experimental results, this observation confirms the reliability of Eq. (11). Consistently with our proposal, conventional materials such as light-weight, fibrous materials (e.g. fibreglass and rockwool) and reticulated foams (e.g. polyurethane and melamine open cell foams) feature porosity and tortuosity very close to unity, whereas other materials tortuosity may assume values well above unity [55].

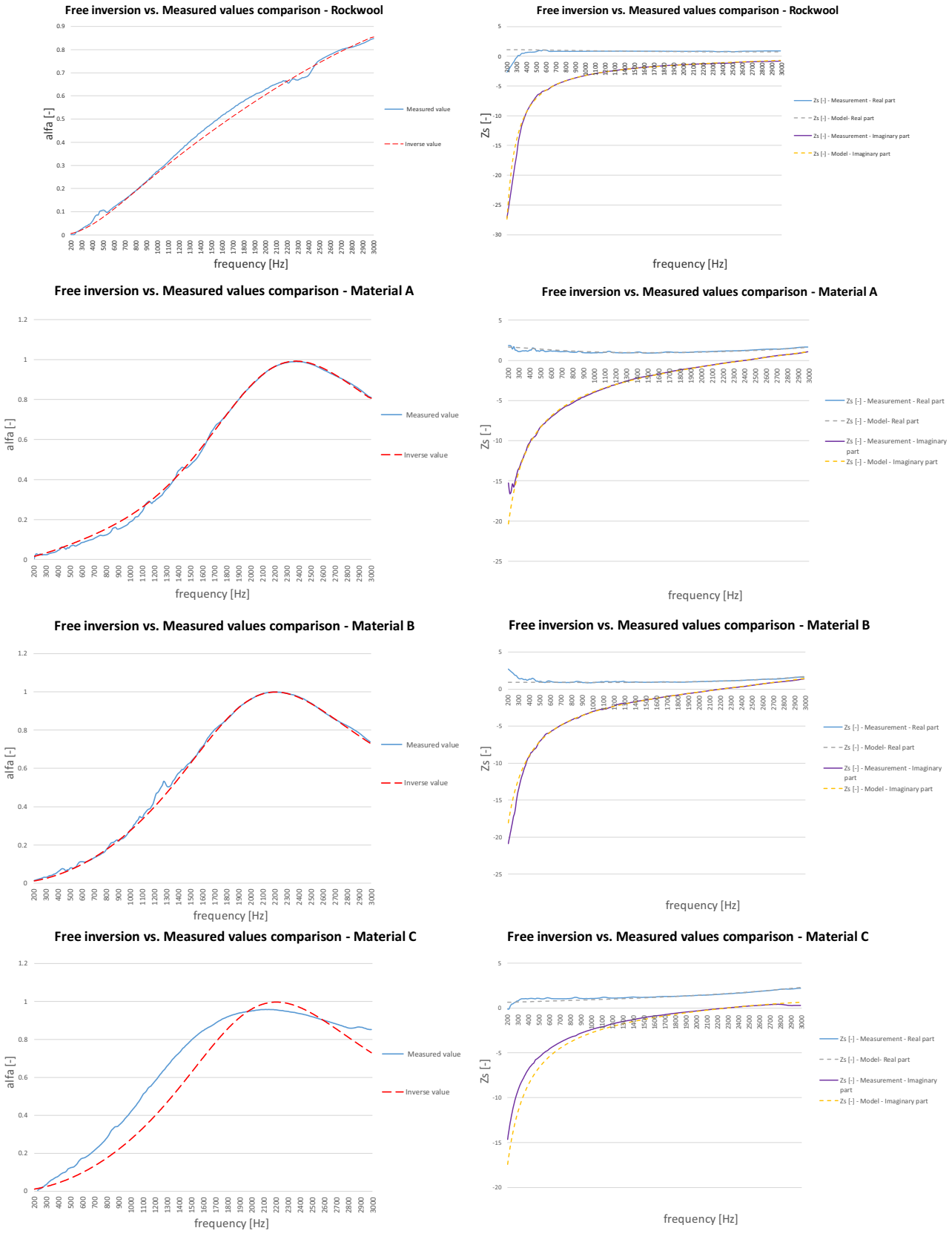

Fig. 8. Comparison of modelled and measured values for rockwool and samples A, B, C and using parameters obtained from the free inversion procedure.

Another very important observation is related to the similarity of the results provided by the modified analytical methods and fixed Λ' value inverse procedure for ϕ, e, α parameters with respect to all three materials: no method manages to calculate with sufficient accuracy the value of the Λ' parameter. Thus, this should be measured with SEM or an equivalent technique to get

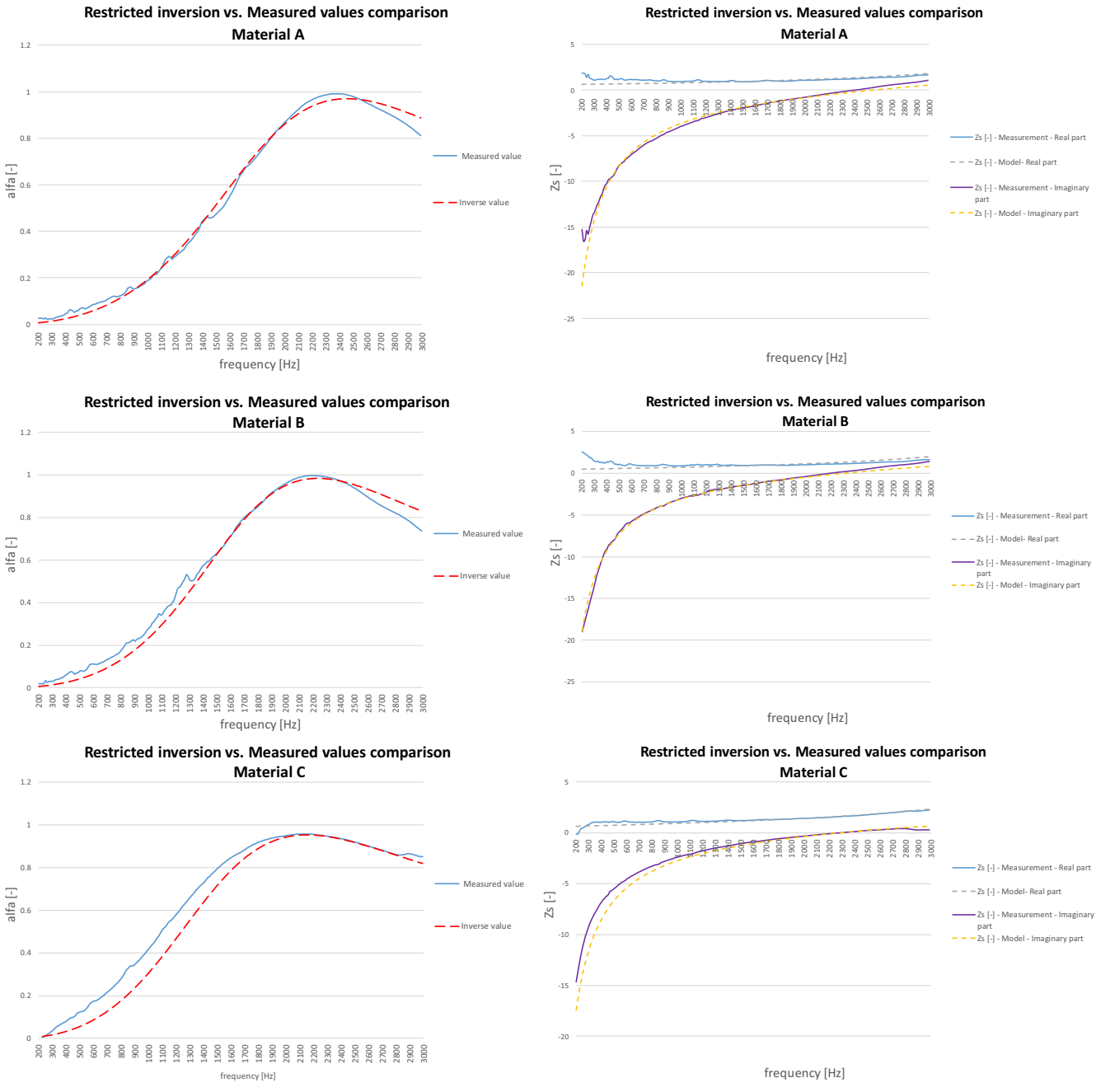

Fig. 9. Comparison of modelled and measured values for samples A, B and C using parameters obtained from the inversion procedure using restricted method (based on analytical model).

a reliable result. This is an important observation as it indicates a direct link between the parameters commonly analyzed and used in the materials science and those used in acoustics.

Both the analytical model (Table 3) and the unrestricted inverse fitting (Table 5, I) lead to an increase of values of this parameter in the sequence A to B to C, while this does not happen for the other two inverse procedures. Whereas this could appears somewhat intriguing, it must be underlined that for our materials a sensitivity analysis [40] revealed that variation of this parameter scarcely affected the goodness of the fit, the most relevant factor being the tortuosity.

The profiles of the sound absorption vs. frequency (Figs. 8–10) show a similar volcano-shape for samples A and B, whereas higher absorption capability is observed for sample C at high frequencies, the decline of the sound absorption being less important.

The tortuosity increases from sample A to sample C (except for analytical model where the value it is almost constant), consistent with an increase of powder concentration and powder weight. This suggests that by increasing the powder content (samples A and B), occlusion of pores might be favored, increasing the tortuosity of the path that the wave must cross through the microstructure.

The pore geometry is associated with viscous and thermal characteristic lengths as illustrated in Fig. 13 [29], showing that the average size of the foam cells is correlated to the thermal characteristic length (~$2\Lambda'$). As for the characteristic viscose length Λ, this parameter can hardly be derived from the microstructural

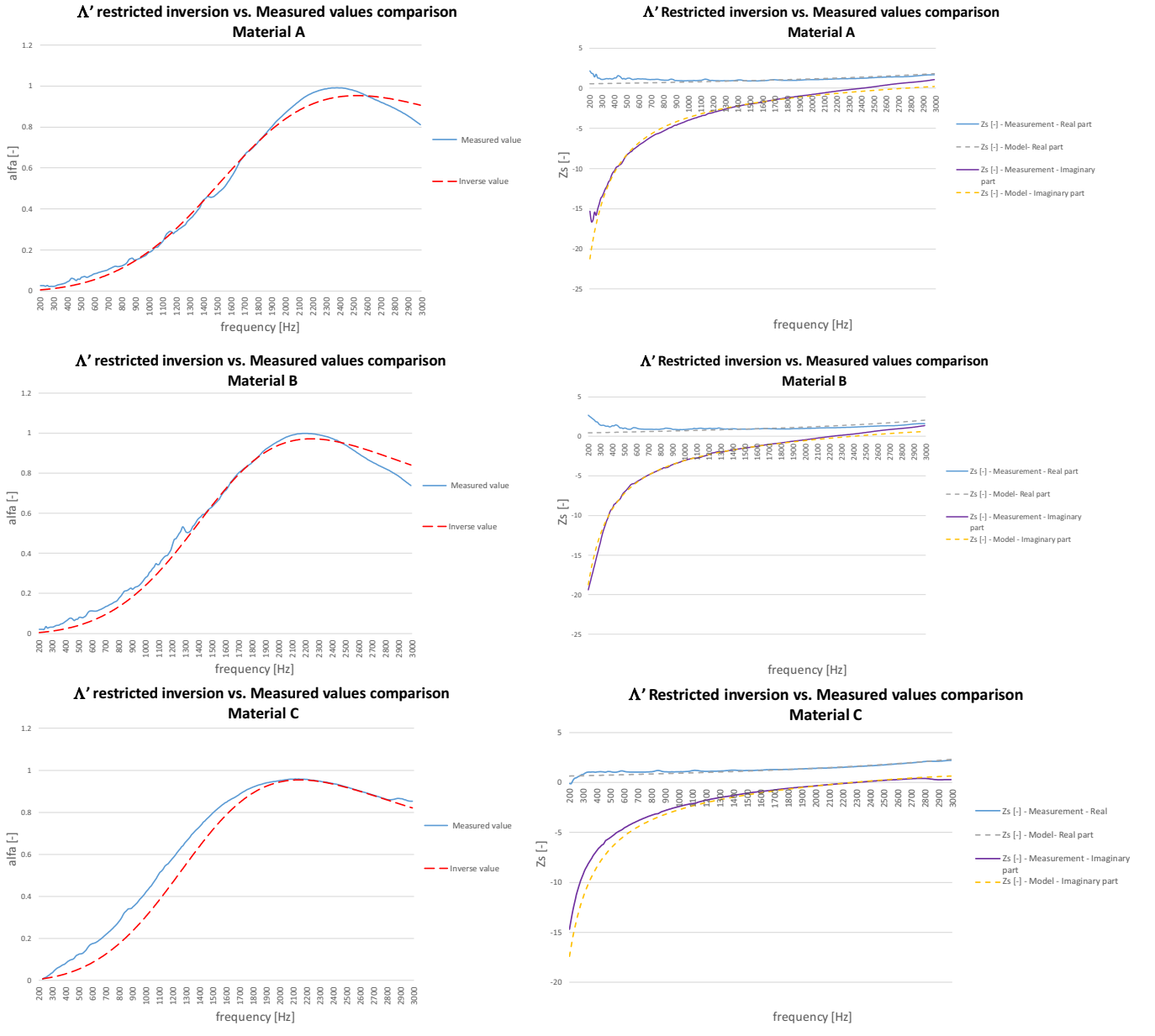

Fig. 10. Comparison of modelled and measured values for samples A, B and C using parameters obtained from the restricted inversion procedure, imposing the measured Λ' value: absorbing coefficient vs. frequency and complex impedance.

Table 5
Parameters obtained from inverse procedure using different fitting approaches.

Material	Flow resistivity (σ)[(N s) m^{-4}]	Porosity (ϕ) [–]	Tortuosity (α) [–]	Viscous characteristic length (Λ) [μm]	Thermal characteristic length (Λ') [μm]	Standard Deviation[a] (σ)
I. Fitting with no restriction						
A	17,744	0.87	6.78	91	194	0.0142
B	34,449	0.96	8.27	128	131	0.0157
C	43,607	0.99	4.78	39	79	0.1018
II. Fitting using restricted method (based on analytical model)						
A	59,676	0.81	4.34	53	53	0.0251
B	40,429	0.92	4.95	53	53	0.0396
C	44,030	0.99	4.76	39	78	0.1017
III. Fitting using experimental pore dimension						
A	59,181	0.82	2.88	29	29	0.0323
B	43,481	0.93	4.11	38	38	0.0385
C	45,312	0.99	4.68	38	75	0.1023

[a] Standard deviation of the calculated α from the experimental values assuming that the latter represent the average value in the range 200–3000 Hz.

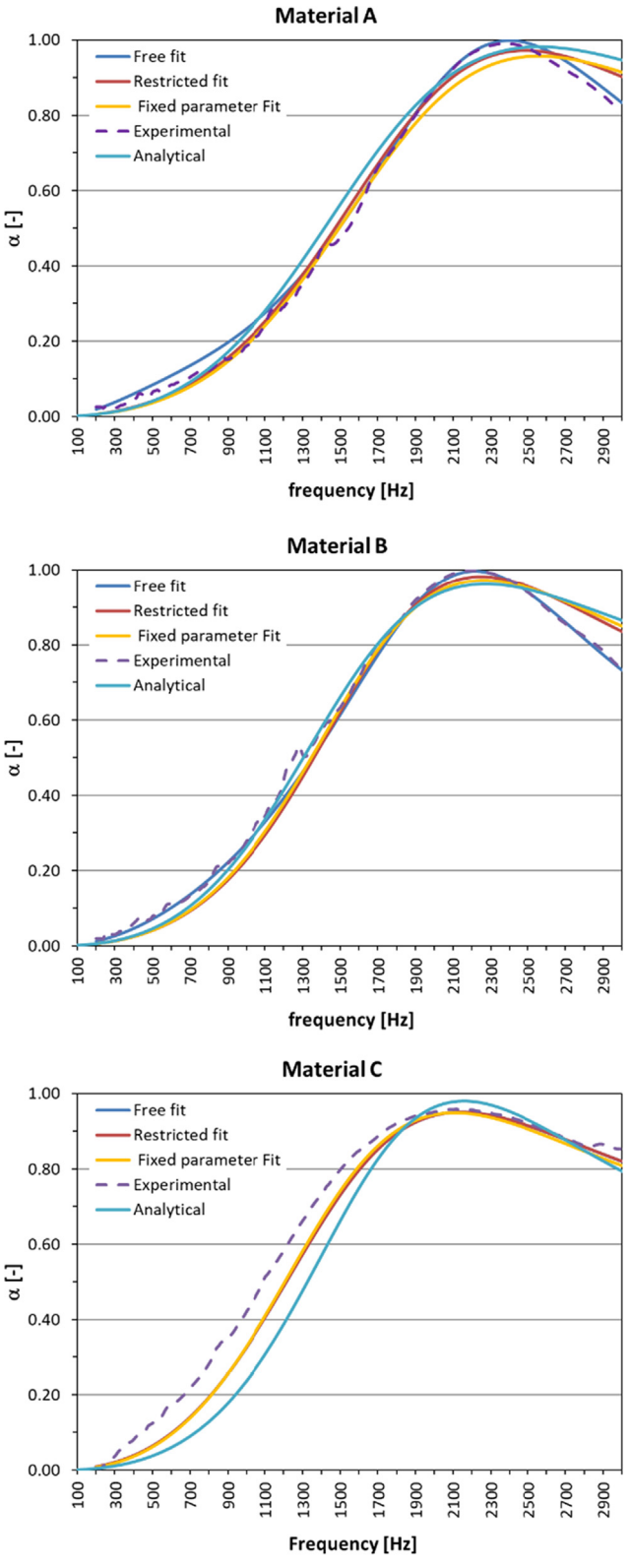

Fig. 11. Comparison expressed as relative % between the TMM calculated frequency trends using inverse procedure results and analytical modified model.

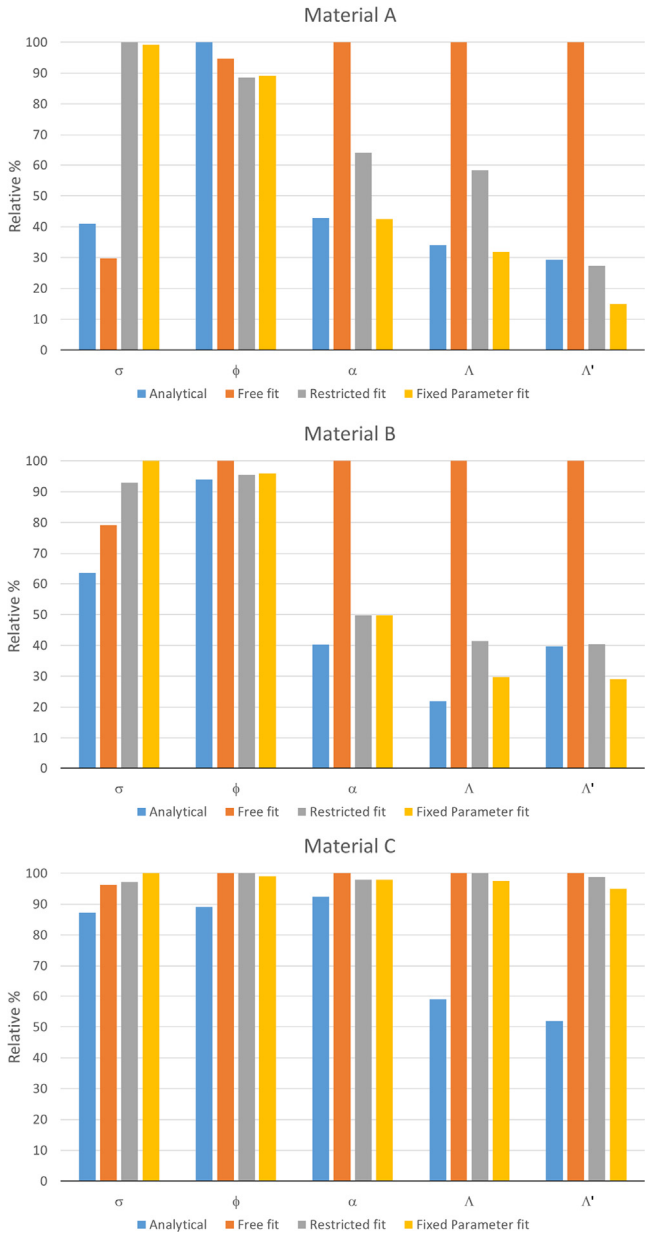

Fig. 12. Comparison of modelled JCA values for samples A, B and C with modified analytical, the inversion techniques: Values are expressed as % of the maximum value observed for each material/parameter.

characterization, whereas its influence is important since narrowing the interconnections between the foam cells, blocks the fluid movement and transition, resulting in improved sound absorption characteristics. The data reported in Tables 4 and 5 for these two parameters suggest a neat effect of the powder addition to the

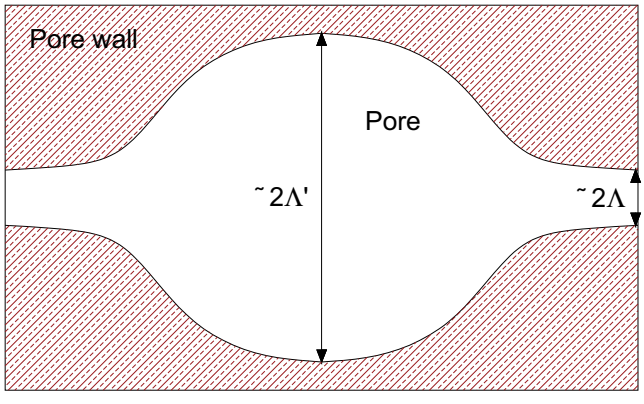

Fig. 13. Pore scheme and indication of thermal characteristic lengths.

synthesis gel: substantial changes in the average dimension of the pores and narrowing the interconnections between them seems to occur, passing from sample A to B and C. As for the similarity of the thermal and viscous characteristic length values, the complex foam cells of our materials feature a parallelepiped interconnected geometry with appears consistent with the similarity of the two parameters.

4. Conclusions

The sound absorbing properties of foam materials are investigated, by means of the laboratory production of three customized cellular alginate foams and applying five different forecasting methods including traditional analytical, a modified analytical with a new proposed equation, and inverse procedures. The acoustic performance was measured and compared with that calculated from the determined acoustic parameters using TMM to assess the reliability of the different procedures.

The analysis of the microstructure of the foams confirm that it has been possible to produce samples with variable controlled morphology, depending on the particle size distribution of the doping powder. Oriented regular cell patterns could be attained by the freeze-drying in the presence of a number of small particles that favors heterogeneous nucleation of ice formation leading to mono-dimensional freezing process. On the contrary, presence of mostly coarse particles leads to an un-oriented cellular sample morphology.

The effects of cell orientation impact the acoustic properties as the un-oriented cell morphology leads to enhanced sound absorption capacity compared to the samples with more regular and oriented morphology.

As regards acoustic modelling, the analytical modelling of the JCA parameters, namely tortuosity, viscous characteristic length, thermal characteristic length, porosity and flow resistivity showed some limitations of the applicability of the traditional equation, because they are strongly related to fibrous materials rather than foams.

For this reason, after the demonstration that this difference may be caused by a wrong theoretical estimation of some parameters, a new equation for the determination of the tortuosity was proposed and validated against experimental data using TMM calculation and inverse parameter determination.

The inverse determination of the physical parameters, using three different fitting procedures was applied to the different foams providing a deeper insight into the behavior of the materials: consistent with SEM microstructural analysis, quite comparable properties were found for Material A and B and somewhat different those for Material C. This assessment allowed to demonstrate that the sound absorbing performance depends on cell shape identified by the thermal lengths results. As a matter of fact, the same foaming agent including different doping powders presents diverse sound absorption trends (volcano-shaped for material A and B with glass powder and flat for material C with fiberglass inclusions, as the decline of the sound absorption being less important).

Finally, the inverse procedure using the thermal characteristic length derived from the SEM micrographs as imposed parameter demonstrated that the analytical obtained values of porosity and the new proposed equation for the determination of the tortuosity are in very good agreement. Moreover, results clearly highlight that the inverse procedure has to be run only with the use of measured values of thermal characteristic length, in order to obtain reliable results directly related to the real microstructure. Thus, a direct link between the materials science property and acoustics has been established.

Author Contributions

M.C. developed the research. M.C. elaborated acoustic data, numerical simulation and acoustic inversions, G.K.d'A. synthetized and characterized the foam samples, J.K. and A.G. overviewed the research. M.C., G.K.d'A. and J.K. wrote the paper.

Declaration of Competing Interest

The authors declare that they have no known competing financial interests or personal relationships that could have appeared to influence the work reported in this paper.

Acknowledgments

This work was financed by "Klimahouse and energy production" in the framework of the programmatic-financial agreement with the Autonomous Province of Bozen-Bolzano of Research Capacity Building, which are gratefully acknowledged.

The authors want to thank Gianluca Turco (Department of Medicine, Surgery and Health Sciences, University of Trieste) for SEM pictures and Andrea Travan (Department of Life Science, University of Trieste) for help in foams production and characterisation. Paolo Bonfiglio of Materiacustica srl is gratefully acknowledged for his precious advices.

References

[1] Asdrubali F, D'Alessandro F, Schiavoni S. A review of unconventional sustainable building insulation materials. Sustain Mater Technol 2015;4:1–17. https://doi.org/10.1016/j.susmat.2015.05.002.

[2] Asdrubali F, Schiavoni S, Horoshenkov KV. A review of sustainable materials for acoustic applications. Build Acoust 2012;19:283–312. https://doi.org/10.1260/1351-010X.19.4.283.

[3] Wi S, Yang S, Berardi U, Kim S. Assessment of recycled ceramic-based inorganic insulation for improving energy efficiency and flame retardancy of buildings. Environ Int 2019;130.. https://doi.org/10.1016/j.envint.2019.06.010.

[4] Wu D, Xu F, Sun B, Fu R, He H, Matyjaszewski K. Design and preparation of porous polymers. Chem Rev 2012;112:3959–4015. https://doi.org/10.1021/cr200440z.

[5] Scheffler M, Colombo P, editors. Cellular ceramics: structure, manufacturing, properties and applications. Weinheim: Wiley-VCH; 2005.

[6] Studart AR, Gonzenbach UT, Tervoort E, Gauckler LJ. Processing routes to macroporous ceramics: a review. J Am Ceram Soc 2006;89:1771–89. https://doi.org/10.1111/j.1551-2916.2006.01044.x.

[7] Colombo P, Bernardo E. Cellular Structures. In: Riedel, R, Chen, I-W (eds.). Ceram Sci Technol, Vol. 1 Struct., vol. 1, Wiley-VCH Verlag GmbH & Co. KGaA; 2008, pp. 407–41. https://doi.org/10.1002/9783527631926.ch10.

[8] Colombo P, Vakifahmetoglu C, Costacurta S. Fabrication of ceramic components with hierarchical porosity. J Mater Sci 2010;45:5425–55. https://doi.org/10.1007/s10853-010-4708-9.

[9] Fernandes HR, Tulyaganov DU, Ferreira JMF. Preparation and characterization of foams from sheet glass and fly ash using carbonates as foaming agents. Ceram Int 2009;35:229–35. https://doi.org/10.1016/j.ceramint.2007.10.019.

[10] Winterton N. Twelve more green chemistry principles. Green Chem 2001;3:G73–5. https://doi.org/10.1039/b110187k.

[11] Dele-Afolabi TT, Hanim MAA, Norkhairunnisa M, Sobri S, Calin R. Research trend in the development of macroporous ceramic components by pore forming additives from natural organic matters: a short review. Ceram Int 2017;43:1633–49. https://doi.org/10.1016/j.ceramint.2016.10.177.

[12] Zhu Y, Romain C, Williams CK. Sustainable polymers from renewable resources. Nature 2016;540:354–62. https://doi.org/10.1038/nature21001.

[13] Kyaw Oo D'Amore G, Caniato M, Travan A, Turco G, Marsich L, Ferluga A, et al. Innovative thermal and acoustic insulation foam from recycled waste glass powder. J Clean Prod 2017;165:1306–15. https://doi.org/10.1016/j.jclepro.2017.07.214.

[14] Lee KY, Mooney DJ. Alginate: properties and biomedical applications. Prog Polym Sci Oxf 2012;37:106–26. https://doi.org/10.1016/j.progpolymsci.2011.06.003.

[15] Goh CH, Heng PWS, Chan LW. Alginates as a useful natural polymer for microencapsulation and therapeutic applications. Carbohydr Polym 2012;88:1–12. https://doi.org/10.1016/j.carbpol.2011.11.012.

[16] Galiano F, Briceño K, Marino T, Molino A, Christensen KV, Figoli A. Advances in biopolymer-based membrane preparation and applications. J Membr Sci 2018;564:562–86. https://doi.org/10.1016/j.memsci.2018.07.059.

[17] Shaari N, Kamarudin SK. Chitosan and alginate types of bio-membrane in fuel cell application: an overview. J Power Sources 2015;289:71–80. https://doi.org/10.1016/j.jpowsour.2015.04.027.
[18] Vincent T, Dumazert L, Dufourg L, Cucherat C, Sonnier R, Guibal E. New alginate foams: Box-Behnken design of their manufacturing; fire retardant and thermal insulating properties. J Appl Polym Sci 2018;135:45868. https://doi.org/10.1002/app.45868.
[19] IUPAC. IUPAC Gold Book – gel. 2019. https://doi.org/10.1351/goldbook.G02600.
[20] Rechberger F, Niederberger M. Synthesis of aerogels: from molecular routes to 3-dimensional nanoparticle assembly. Nanoscale Horiz 2017;2:6–30. https://doi.org/10.1039/c6nh00077k.
[21] Plieva FM, Kirsebom H, Mattiasson B. Preparation of macroporous cryostructurated gel monoliths, their characterization and main applications. J Sep Sci 2011;34:2164–72. https://doi.org/10.1002/jssc.201100199.
[22] Mahler W, Bechtold MF. Freeze-formed silica fibres. Nature 1980;285:27–8. https://doi.org/10.1038/285027a0.
[23] Zhang H, Cooper AI. Aligned porous structures by directional freezing. Adv Mater 2007;19:1529–33. https://doi.org/10.1002/adma.200700154.
[24] Porrelli D, Travan A, Turco G, Marsich E, Borgogna M, Paoletti S, et al. Alginate-hydroxyapatite bone scaffolds with isotropic or anisotropic pore structure: material properties and biological behavior. Macromol Mater Eng 2015;300:989–1000. https://doi.org/10.1002/mame.201500055.
[25] Lind-Nordgren E, Göransson P. Optimising open porous foam for acoustical and vibrational performance. J Sound Vib 2010;329:753–67. https://doi.org/10.1016/j.jsv.2009.10.009.
[26] Biot MA. Theory of propagation of elastic waves in a fluid-saturated porous solid II. Higher frequency range. J Acoust Soc Am 1956;28:179–91. https://doi.org/10.1121/1.1908241.
[27] Biot MA. Theory of propagation of elastic waves in a fluid-saturated porous solid. I low-frequency range. J Acoust Soc Am 1956;28:168–78. https://doi.org/10.1121/1.1908239.
[28] Biot MA. Mechanics of deformation and acoustic propagation in porous media. J Appl Phys 1962;33:1482–98. https://doi.org/10.1063/1.1728759.
[29] Johnson DL, Koplik J, Dashen R. Theory of dynamic permeability and tortuosity in fluid-saturated porous media. J Fluid Mech 1987;176:379. https://doi.org/10.1017/S0022112087000727.
[30] Champoux Y, Allard J. Dynamic tortuosity and bulk modulus in air-saturated porous media. J Appl Phys 1991;70:1975–9. https://doi.org/10.1063/1.349482.
[31] Panneton R. Comments on the limp frame equivalent fluid model for porous media EL217–EL222. J Acoust Soc Am 2007;122. https://doi.org/10.1121/1.2800895.
[32] Kino N. Further investigations of empirical improvements to the Johnson–Champoux–Allard model. Appl Acoust 2015;96:153–70. https://doi.org/10.1016/j.apacoust.2015.03.024.
[33] Sadouki M. Experimental characterization of rigid porous material via the first ultrasonic reflected waves at oblique incidence. Appl Acoust 2018;133:64–72. https://doi.org/10.1016/j.apacoust.2017.12.010.
[34] Caniato, M, Travan, A. Method for recycling waste material. EP 3216825, 2016.
[35] Zhang YS, Khademhosseini A. Advances in engineering hydrogels. Science 2017;356. https://doi.org/10.1126/science.aaf3627.
[36] Travan A, Pelillo C, Donati I, Marsich E, Benincasa M, Scarpa T, et al. Non-cytotoxic silver nanoparticle-polysaccharide nanocomposites with antimicrobial activity. Biomacromolecules 2009;10:1429–35. https://doi.org/10.1021/bm900039x.
[37] Travan A, Scognamiglio F, Borgogna M, Marsich E, Donati I, Tarusha L, et al. Hyaluronan delivery by polymer demixing in polysaccharide-based hydrogels and membranes for biomedical applications. Carbohydr Polym 2016;150:408–18. https://doi.org/10.1016/j.carbpol.2016.03.088.
[38] Fotsing ER, Dubourg A, Ross A, Mardjono J. Acoustic properties of periodic micro-structures obtained by additive manufacturing. Appl Acoust 2019;148:322–31. https://doi.org/10.1016/j.apacoust.2018.12.030.
[39] Tarnow V. Airflow resistivity of models of fibrous acoustic materials. J Acoust Soc Am 1996;100:3706–13. https://doi.org/10.1121/1.417233.
[40] Bonfiglio P, Pompoli F. Inversion problems for determining physical parameters of porous materials: overview and comparison between different methods. Acta Acust United Acust 2013;99:341–51. https://doi.org/10.3813/AAA.918616.
[41] Bonfiglio P, Pompoli F, Shravage P. Quasistatic evaluation of mechanical properties of poroelastic materials: static and dynamic strain dependence and in vacuum tests 3037 3037. J Acoust Soc Am 2008;123. https://doi.org/10.1121/1.2932705.
[42] Olivas GI, Barbosa-Cánovas GV. Alginate–calcium films: water vapor permeability and mechanical properties as affected by plasticizer and relative humidity. LWT Food Sci Technol 2008;41:359–66. https://doi.org/10.1016/j.lwt.2007.02.015.
[43] Scognamiglio F, Travan A, Borgogna M, Donati I, Marsich E, Bosmans JWAM, et al. Enhanced bioadhesivity of dopamine-functionalized polysaccharidic membranes for general surgery applications. Acta Biomater 2016;44:232–42. https://doi.org/10.1016/j.actbio.2016.08.017.
[44] Scognamiglio F, Travan A, Donati I, Borgogna M, Marsich E, Andersen T, et al. H2O2 causes improved adhesion between a polysaccharide-based membrane and intestinal serosa. Colloids Interface Sci Commun 2016;15:5–8. https://doi.org/10.1016/j.colcom.2016.11.002.
[45] Verdejo R, Stämpfli R, Alvarez-Lainez M, Mourad S, Rodriguez-Perez MA, Brühwiler PA, et al. Enhanced acoustic damping in flexible polyurethane foams filled with carbon nanotubes. Compos Sci Technol 2009;69:1564–9. https://doi.org/10.1016/j.compscitech.2008.07.003.
[46] Oliveux G, Dandy LO, Leeke GA. Current status of recycling of fibre reinforced polymers: review of technologies, reuse and resulting properties. Prog Mater Sci 2015;72:61–99. https://doi.org/10.1016/j.pmatsci.2015.01.004.
[47] Overcash M, Twomey J, Asmatulu E, Vozzola E, Griffing E. Thermoset composite recycling – driving forces, development, and evolution of new opportunities. J Compos Mater 2018;52:1033–43. https://doi.org/10.1177/0021998317720000.
[48] Zhang H, Hussain I, Brust M, Butler MF, Rannard SP, Cooper AI. Aligned two- and three-dimensional structures by directional freezing of polymers and nanoparticles. Nat Mater 2005;4:787–93. https://doi.org/10.1038/nmat1487.
[49] Li WL, Lu K, Walz JY. Freeze casting of porous materials: review of critical factors in microstructure evolution. Int Mater Rev 2012;57:37–60. https://doi.org/10.1179/1743280411Y.0000000011.
[50] Deville S. Freeze-casting of porous ceramics: a review of current achievements and issues. Adv Eng Mater 2008;10:155–69. https://doi.org/10.1002/adem.200700270.
[51] Deville S, Maire E, Lasalle A, Bogner A, Gauthier C, Leloup J, et al. Influence of particle size on ice nucleation and growth during the ice-templating process. J Am Ceram Soc 2010;93:2507–10. https://doi.org/10.1111/j.1551-2916.2010.03840.x.
[52] Deville S, Saiz E, Tomsia AP. Ice-templated porous alumina structures. Acta Mater 2007;55:1965–74. https://doi.org/10.1016/j.actamat.2006.11.003.
[53] Archie GE. The electrical resistivity as an aid in core analysis interpretation. Trans Am Inst Min Metall Eng 1942;146:54–62.
[54] Allard J, Atalla N. Propagation of sound in porous media modelling sound absorbing materials. 2nd ed. London: Wiley; 2009.
[55] Horoshenkov KV. A review of acoustical methods for porous material characterisation. Int J Acoust Vib 2017;22.. https://doi.org/10.20855/ijav.2017.22.1455.